

Experimental realisation of a non-deterministic optical noiseless amplifier

Franck Ferreyrol, Rémi Blandino, Marco Barbieri, Rosa Tualle-Brouri, and Philippe Grangier.

*Groupe d'Optique Quantique, Laboratoire Charles Fabry, Institut d'Optique, CNRS,
Université Paris-Sud, Campus Polytechnique, RD 128, 91127 Palaiseau cedex, France*

Linear amplifiers are necessarily affected by a minimal amount of noise, which is needed in order to preserve the linearity and the unitarity prescribed by quantum mechanics. Such a limitation might be partially overcome if the process is realised by conditioning its operation on a trigger event, for instance the result of a measurement. Here we present a detailed analysis of a noiseless amplifier, implemented using linear optics, a down-conversion based single-photon source, and single-photon detection. Our results demonstrate an amplification adding a level of noise lower than the minimal allowed by quantum mechanics for deterministic amplifiers. This is made possible by the non-deterministic character of our device, whose success rate is sufficiently low not to violate any fundamental limit. We compare our experimental data to a model taking into account the main imperfections of the setup, and find a good agreement.

I. INTRODUCTION

The classical description of a linear amplifying device uses two key parameters: its gain and its added noise. To some extent, these two parameters are independent, and one can imagine a device working at an arbitrary large gain with an arbitrarily small noise. However, the classical picture does not tell us the full story, and fundamental limitations appear when looking at the quantum aspects of the process. Then, the amplification of an arbitrary signal does affect its fluctuation properties, depending on the effective gain of the device [1]. This can be understood by noticing that a noiseless deterministic phase independent amplifier would allow to improve the initial signal-to-noise ratio on an input beam, and eventually to violate Heisenberg's inequalities. In a more rigorous framework, one can observe that it is necessary to introduce an extra noise operator so that the output field can satisfy the canonical commutation relations.

These limitations can be partially overcome if we renounce to a deterministic implementation. The idea is to achieve noiseless amplification only for a fraction of the total events, with a success probability low enough not to increase the net information. In this case, we need a suitable triggering mechanism able to sort the successful events from the whole ensemble.

Several proposals have been presented to realise probabilistic noiseless amplification [2–4]. The present paper is devoted to the device proposed in [2], based on a variation of the teleportation protocol, with a detailed analysis of its experimental realisation [5] and of the theoretical model used to describe the data.

This work is organised as follows. In Section II we give a brief review of the fundamental concepts about the amplification of quantum signals. In Section III we detail our experimental setup and present a simple theoretical model. Section IV discusses the results, and finally conclusions and perspectives are presented in Section V.

II. AMPLIFICATION OF QUANTUM SIGNALS

A. General framework

Coherent states have been introduced by Roy Glauber as the translation into quantum language of states exhibiting quasi classical properties [6]. Their classicality manifests in the fact that for large average photon number, one can define almost perfectly an amplitude and a phase, as for classical fields. However, at weaker intensities quantum features are predominant, hence their application to quantum cryptography [7]. This approach to quantum key distribution somehow bridges between classical and quantum communications, as it exploits quantum characteristics of laser pulses which can be easily transmitted over ordinary channels. At difference with classical communication, adopting an amplifier in order to recover losses from the transmission is not a winning strategy under several aspects [8]. The main drawback is that amplification does affect the fluctuation properties of coherent states, corrupting their property of being minimal uncertainty packets, which is crucial for their use in quantum cryptography.

To illustrate this, we recall the treatment of a quantum amplifier presented by Caves in [1]. Consider an optical field, whose quadratures are defined as:

$$\begin{aligned} X &= \sqrt{N_0}(a^\dagger + a), \\ P &= i\sqrt{N_0}(a^\dagger - a), \end{aligned} \tag{1}$$

where a^\dagger and a are the creation and destruction operators, respectively, and N_0 is a constant including normalisation factors. In these terms, Heisenberg relation writes: $[X, P] = 2iN_0$. We show in Fig.1a a contour plot for the case of coherent states, relevant to our investigation. An ideal amplifier would perform the transformation $X \rightarrow g_X X, P \rightarrow g_P P$, where we allowed the gain to be phase dependent by introducing two distinct values g_X, g_P . In general, this transformation does not produce physically meaningful quadratures, as they do not satisfy the uncertainty relation. It is then necessary to introduce

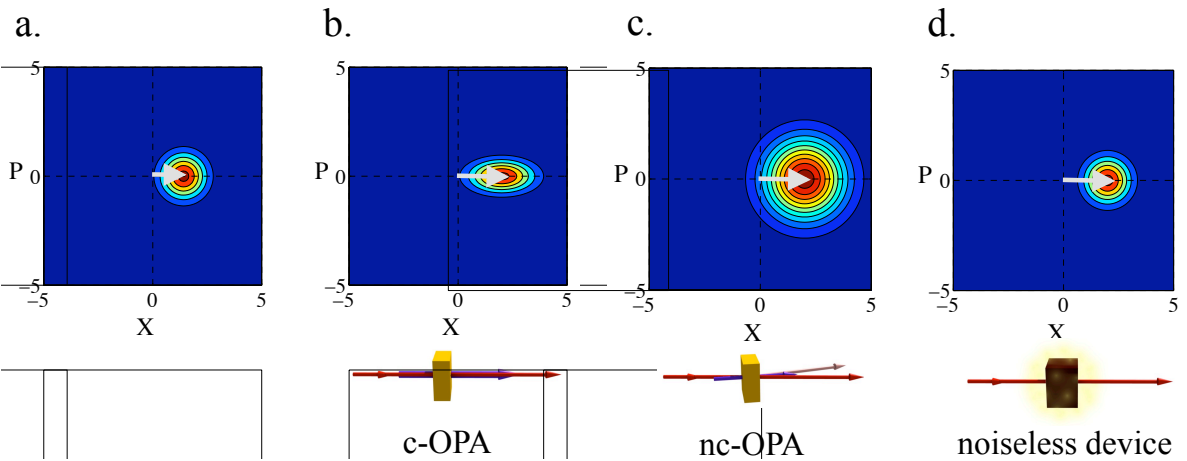


Figure 1: Amplification of coherent states. The quantum states are shown as a contour plots in the phase space. a) The initial coherent state with variance one and amplitude $\alpha = 1$. b) Phase-dependent amplification. In this case, only the X quadrature is amplified by a factor g , while its conjugate P is de-amplified by $1/g$. Variances are modified accordingly, so that the amplification does not lead to a better (nor worse) resolution in X . This process results from a passage in a collinear optical parametric amplifier (c-OPA). c) Phase-independent amplification. The gain g is the same for all quadratures, consequently the round shape is preserved. Nevertheless the resolution is worse than the initial case due to excess noise. This operation can be realised by tuning an OPA in a non-collinear regime (nc-OPA). d) Noiseless amplifier. The input amplitude is increased for any value of its phase, without affecting its noise properties.

two auxiliary noise fields B_X, B_P :

$$\begin{aligned} X_{\text{out}} &= g_X X_{\text{in}} + B_X, \\ P_{\text{out}} &= g_P P_{\text{in}} + B_P. \end{aligned} \quad (2)$$

The noise fields average to zero and they need to satisfy:

$$[B_X, B_P] = 2iN_0(g_X g_P - 1). \quad (3)$$

For a phase-dependent amplifier, the excess noise may vanish if $g_X = 1/g_P$. This does not imply, however, that the amplification is noiseless: the gain also enhances quantum fluctuations by a factor g_X^2 . What the device actually does preserve is the initial signal-to-noise ratio (SNR) of the input field (Fig.1b). For a phase-independent amplifier, $g_X = g_P = g$, and an excess noise contribution of $(g^2 - 1)$ vacuum units appears. The SNR is worsened during the amplification process (Fig.1c).

Comparing these two situations, a phase-dependent amplifier is often called “noiseless”, in the sense that it adds no excess noise, as compared to the phase-independent case. However, throughout this paper we will reserve this term only to an ideal amplifier that would strictly preserve the noise property of the input for both quadratures (Fig.1d): such a device is thus forbidden within the framework of eqs. (2) and (3).

B. The noiseless amplifier

In order to overcome the bound (3) and realise a noiseless process, we can take inspiration to the linear optical approach to quantum computing, as proposed by Knill, Laflamme and Milburn (KLM) [9].

When measurements come into play, an initial state $|\psi_{\text{in}}\rangle$ is not necessarily linked to the resulting output $|\psi_{\text{out}}\rangle$ by a unitary evolution. The pivot in KLM scheme is to exploit this to simulate Kerr-like interaction between two photons using uniquely linear elements. To do so, some extra resources need to be brought in: these have to interact linearly with the target photons, then subsequently they are measured. The output is observed only when a particular measurement result occurs, and other events are discarded. We could possibly design a similar scheme to create an extremely nonlinear effect such as the one needed for noiseless amplification.

The first proposal in this sense has been put forward by Ralph and Lund, based on a variant of teleportation; as said above, our implementation is a direct realisation of their protocol. Different schemes adopt either mixing with a thermal state and photon subtraction [4], or sequences of photon addition and subtraction [3]. The conceptual scheme is shown in Fig.2a. For the moment, we restrict our attention to weak intensities coherent states ($\|\alpha\| \ll 1$), which can be well approximated by a development up to the single-photon term:

$$|\alpha\rangle \simeq |0\rangle + \alpha|1\rangle. \quad (4)$$

The ancillary resource needed to accomplish the task is a single photon state $|1\rangle$. This photon is split on an asymmetric beam splitter (A-BS) with reflectivity r , generating an entangled state:

$$\sqrt{1-r^2}|1\rangle_T|0\rangle_R + r|0\rangle_T|1\rangle_R, \quad (5)$$

where T, R denote the output modes of the A-BS. The T mode represents the output port of the amplifier. The

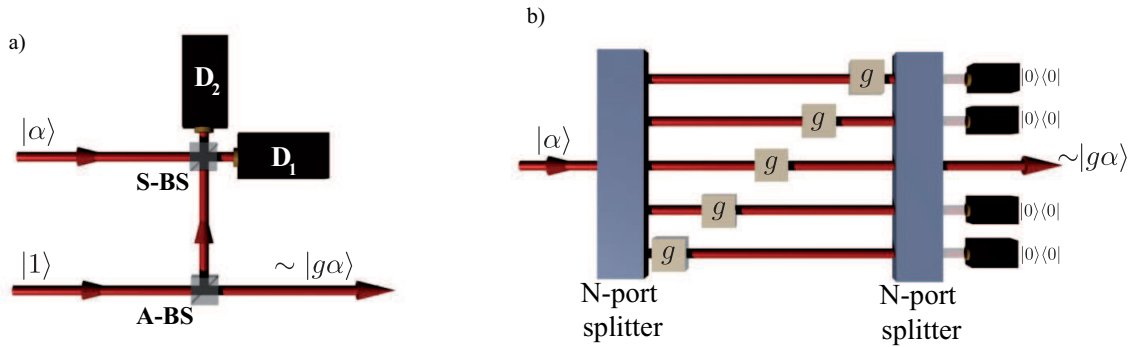


Figure 2: Teleportation-based noiseless amplifier. a) Single-stage amplifier for $\|\alpha\| \ll 1$. A single photon is split on an asymmetric beamsplitter (A-BS). The input state $|\alpha\rangle$ is superposed with reflected output of the A-BS on asymmetric beamsplitter (S-BS). A successful run is flagged by a single photon event on detector D_1 and no photons on detector D_2 , or viceversa. The transmitted mode is the output of the amplifier, and, conditioned on the right detection events, it is approximately in the amplified state $|g\alpha\rangle$. b) Multi-stage amplifier for arbitrary intensities. The input is divided into N equal parts, each of them having an acceptable intensity to be amplified in a single stage, depicted as boxes labelled g . The N outputs are then recombined, and the run is accepted only if no photons are detected on the remaining $N-1$ ports.

input state is made interfere with the R mode on a symmetric beam splitter (S-BS), then photon counting is performed at the out-ports. We accept the run when a single photon is measured by the detector D_1 and no photons arrive on the detector D_2 . This event can arise from two distinct occurrences: either the single photon came from the entangled state, then the vacuum is left on the T mode, or the single photon came from the input, thus a single photon is present on the T mode. Quantum interference generates the state:

$$|0\rangle + g\alpha|1\rangle, \quad (6)$$

with $g = \sqrt{1 - r^2}/r > 1$ acting as a gain factor. If the condition $g\|\alpha\| \ll 1$ is satisfied, the superposition (6) is still an adequate approximation of the coherent state $|g\alpha\rangle$, resulting in the implementation of the noiseless amplifier. Conditioning on the event when one photon is detected by D_2 and vacuum by D_1 also results in a successful run, up to a π phase shift on the single photon component. Both events are acceptable if active phase modulation is applied.

For arbitrary input intensities, we can imagine to split $|\alpha\rangle$ on a N -port beam splitter in such a way that $\|\alpha\|/\sqrt{N}$ is sufficiently weak. Each portion is then amplified by the device described above, and the outputs are recombined on a second N -port splitter, Fig. 2b. As the output states are not exactly coherent states, it is necessary to ensure that all the radiation emerges from a single port. The success probability $P = r^{2N} \exp(-(g^2 - 1)\|\alpha\|^2)$ becomes exponentially small as $\|\alpha\|$ increases, preventing any overall information gain.

The protocol can be interpreted as a variant of the teleportation scheme adopted for the “quantum scissors” [10, 11], which correspond to the case $r^2 = 1/2$. It was originally proposed with the aim of truncating a coherent state to its single photon component so to generate an optical qubit. It retains the main features of the telepor-

tation scheme by the use of an entangled resource – the split single photon – and a joint measurement, obtained from interference on the S-BS and photon counting. The working principle of the amplifier is indeed to teleport the information coded in the input coherent state – e.g. its phase and amplitude – to a more intense beam.

C. Gain and noise figures

In our implementation, we will consider the amplitude (measured from the origin) as the signal. This suggests to quantify the amplification by an effective gain g_{eff} defined as the ratio of the output and input mean values:

$$g_{\text{eff}} = \frac{\langle X_{\text{out}} \rangle}{\langle X_{\text{in}} \rangle}, \quad (7)$$

where without restriction of generality we have defined the X axis along the direction of the input.

Actual implementations of a noiseless amplifier will be unavoidably affected by non ideal components, resulting in some excess noise. We then need an indicator to compare the noise at the input and at the output while taking into account the amplification. A suggestion in this sense comes from electronics and from quantum non-demolition measurements [7, 12–14]. The question to be asked is what level of noise should we add to the input to find the one actually observed at the output, were we operating a noiseless device. The quantity

$$N_{\text{eq}} = \frac{\langle \delta X_{\text{out}}^2 \rangle}{g^2} - \langle \delta X_{\text{in}}^2 \rangle, \quad (8)$$

called “equivalent input noise” relates according to this picture the variance of the output state $\langle \delta X_{\text{out}}^2 \rangle$ to the initial variance $\langle \delta X_{\text{in}}^2 \rangle$ and the gain g . Here N_{eq} is defined for the X quadrature, but the definition can be extended to any arbitrary direction of the phase space.

In the case of a usual phase-dependent amplifier for the X quadrature, the variance at the output is proportional to the one at the input $\langle \delta X_{\text{out}}^2 \rangle = g_X^2 \langle \delta X_{\text{in}}^2 \rangle$: N_{eq} vanishes, meaning that the initial fluctuation properties are preserved as said above [15, 16]. For the phase-independent device, one has $N_{\text{eq}} = |g^2 - 1|/g^2$, hence some excess noise is introduced in the process. This holds true if we allow for $g < 0$, i.e. a beam splitter with transmittivity g : even if the fluctuation properties for a coherent state are left untouched, N_{eq} is useful to flag a reduction in resolution due to losses.

The ideal case for the noiseless amplifier shows $N_{\text{eq}} = (1 - g^2)/g^2 < 0$: the device acts as a kind of noise eater for the input state. This condition can not be met by any deterministic device, therefore we can use the criterion $N_{\text{eq}} < 0$ as the distinctive feature of a noiseless amplification process, even if it is non-ideal.

III. THE EXPERIMENT

A. Description of the setup

While the implementation of the general device is a technical challenge, a single stage noiseless amplifier is well within the present experimental possibilities. This study goes beyond an academic exercise, given the interest of weak coherent states for quantum cryptography [17]. In our investigation, we also aim to establish experimentally what is the maximal useful value of $\|\alpha\|$ one can feed in the amplifier without being severely affected by the abrupt truncation (6).

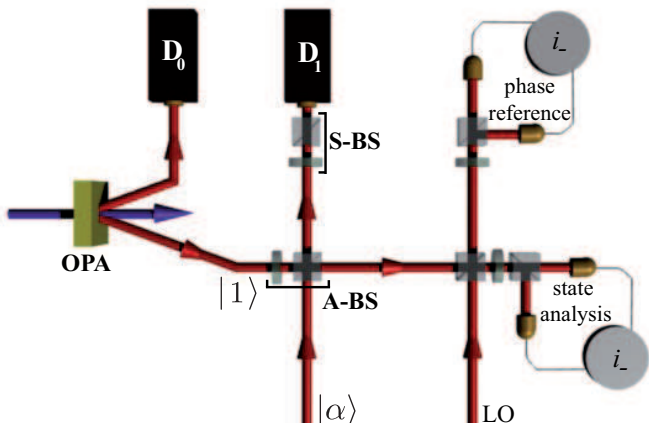


Figure 3: Diagram of the experimental setup. We used single photons produced by an optical parametric amplifier (OPA), which is then split over two polarisation modes by the A-BS, realised with a half-wave plate (HWP) and a polariser. This is recombined with the input $|\alpha\rangle$ on the S-BS, realised again by a HWP and a polariser. The output state is analysed by homodyne detection, using a phase reference coherent with the input. See text for more detail.

The scheme of our setup is shown in Fig. 3. Single

photons are produced by using a non-linear crystal an optical parametric amplifier (OPA). This process generates photon pairs in two correlated modes; the presence of a single photon on one mode is inferred by a click on a single photon detector D_0 placed on the other “twin” mode [18]. The source is a $100\mu\text{m}$ thick KNbO_3 slab, pumped by doubled Ti:Sa laser pulses ($P_{\text{max}}=3.3\text{mW}$, $\lambda_p = 423.5\text{nm}$, $\Delta t = 220\text{fs}$, repetition rate 800kHz). Phase-matching is temperature-tuned to obtain frequency degenerate emission at an angle $\sim 3^\circ$. Photons on the heralding mode are filtered by a single-mode fibre and a grating-slit assembly transmitting over a bandwidth $\sim 1\text{nm}$ centred on degeneracy $\lambda=2\lambda_p$.

In order to preserve phase stability without active locking, we realised a polarisation encoding of the T and R modes, corresponding to the horizontal (H) and vertical (V) components, respectively. This allows us to realise the A-BS by the combination of a half-wave plate (HWP) and a polarising beam splitter (PBS): the polarisation is prepared in the state $r|V\rangle + \sqrt{1-r^2}|H\rangle$, then the photon is split over two spatial modes.

The input is fed through the second input port of the PBS: its H component represents the coherent input $|\alpha\rangle$ to be amplified, the V component is a phase reference. In this way, both the coherent state and the split single photon are on the same spatial R mode, but with orthogonal polarisations. We can now make these two interfere by a HWP and a PBS, set to implement the S-BS. In the ideal case, we would have one detector on each output of the PBS; due to the limited efficiency of our single-photon detection ($\sim 10\%$), D_2 can be dropped from the actual implementation without significantly affecting the performance of the amplifier. Hence, our device works conditionally on a coincidence count between D_0 and D_1 .

On the T mode we have both the actual output of the amplifier and the reference signal. We can perform homodyne measurements on both polarisation modes [20], so to obtain the quadratures of the output state on H , and a sorting signal on V . The latter gives us the instantaneous value of the phase of the coherent state $|\alpha\rangle$, hence the measured quadrature. Data from the H detection are thus sorted accordingly, which amounts to choose α to be real and positive. The extinction ratio of used polarising cubes, around 10^{-4} , is sufficiently low in order to have negligible effects, provided that the difference of amplitude between the coherent state and the reference signal does not become too important.

B. Modelling of the experiment

The components used in the experiment present several departures from the ideal behaviour, which will affect the output. In order to take into account these imperfections, we adopt the methods developed in [18, 19]. Our treatment is split in two steps: first we compute the actual state produced by our single-photon source, then we feed it as the ancilla for the noiseless amplifier. The con-

ceptual layout is shown in Fig.4.

Concerning the source, two mode squeezing ideally occurs with a gain $\cosh^2(s)$ which depends on the pump power. In the actual OPA, there occurs parasite processes that cause excess noise to appear on these modes. This effect can be modelled by two fictitious squeezers with gain $\cosh^2(\gamma s)$, where γ is the relative strength of the two squeezers. These are represented in transparency in Fig.4.

The quality of our single-photon resource is also limited by heralding. Indeed, this is also performed with a limited efficiency: in a fraction ξ of the events, we detect the correct mode, which will be correlated with the mode of the local oscillator. The remaining cases represent a background of spurious events, whose detection does not affect the other mode. Due to low detection efficiency μ , we can substitute the exact expression of the detection operator with the annihilation operator \hat{a} . The expression of the state conditionally prepared by our OPA is then [18]:

$$W_1(x, p) = \frac{1}{\pi} \left(1 - \delta + \delta \frac{x^2 + p^2}{\sigma^2} \right) e^{-\frac{x^2 + p^2}{\sigma^2}}, \quad (9)$$

where

$$\begin{aligned} \sigma^2 &= 2\eta(\cosh^2(s)\cosh^2(\gamma s) - 1) + 1, \\ \delta &= \frac{2\xi\eta}{\sigma^2} \frac{\sinh^2(s)\cosh^2(\gamma s)}{1 - \operatorname{sech}^2(s)\operatorname{sech}^2(\gamma s)}, \end{aligned} \quad (10)$$

and η is the efficiency of the homodyne detector, HD. We have adopted the convention $N_0 = 1/2$ corresponding to $[X, P] = i$. This expression is valid in the limit of low efficiency of the heralding APD, as it is the case for our experiment, but gives satisfactory numerical results in the general case [18]. The state is characterised by two parameters σ and δ , which can be extracted directly from the quadrature histograms [18].

We now turn our attention to the noiseless amplifier. When conditioning is considered, we have to take into account finite mode matching between the single photon mode, and the coherent state, as this can be achieved with finite precision. The description of the input then needs two different modes: one which is indistinguishable from the one of the single photon $\hat{a}_{//}$, and a second in the orthogonal subspace \hat{a}_{\perp} . The mode of the coherent state has contributions from both subspaces $\hat{a}_{\alpha} = \sqrt{\varepsilon}\hat{a}_{//} + \sqrt{1-\varepsilon}\hat{a}_{\perp}$. The parameter $\varepsilon \sim 1$ quantifies the quality of the interference occurring at S-BS. In order to simplify our calculations, we can rescale the detection efficiency μ of the second APD as $\nu = \mu/\eta$, by considering loss η on the mode \hat{a}_{α} . This creates a symmetry for the two arms of the S-BS, thus simplifies the treatment. We are then working with these two state in our amplifier:

- the single photon state (9);

- a coherent state with an effective amplitude $\alpha_{\text{eff}} = \sqrt{\eta}\sqrt{\varepsilon}\alpha$.

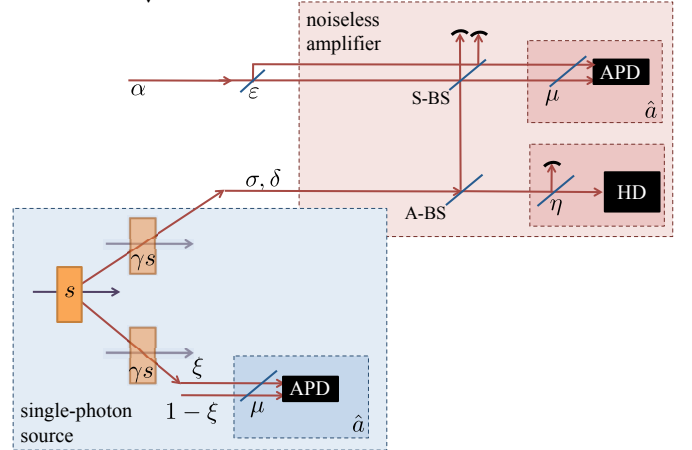


Figure 4: Modelling of the experiment. The imperfections of our set up are taken into account by a series of linear elements, which allow us to calculate an explicit expression for the Wigner function of the output state. Symbols are explained in the text.

This is the starting point for the modelisation of the amplifier. The first step consist in mixing the single photon with the vacuum $W_0(x_0, p_0)$ on the A-BS, having transmittivity t , and reflectivity r :

$$W_{\text{ABS}}(x, p, x_0, p_0) = W_1(tx - rx_0, tp - rp_0)W_0(rx + tx_0, rp + tp_0). \quad (11)$$

We now make the reflected mode interfere with the coherent state on the S-BS, and then trace over the mode we are not observing. This gives a more complex expression $W_{\text{SBS}}(x, p, x_1, p_1)$ describing the output mode (x, p) , and the mode (x_1, p_1) arriving on the APD. As above, detection on the latter is represented by the application of the \hat{a} operator. The final state we obtain correspond to a good conditioning event. However, imperfect matching results in uncorrelated events, very much as it is the case for the modal purity ξ in the single photon state (9). An effective modal purity ξ_{eff} has to be introduced to weight the two contributions:

$$\xi_{\text{eff}} = \frac{P_{//}}{P_{//} + P_{\perp}}, \quad (12)$$

where $P_{//}$ (P_{\perp}) is the probability of detecting one photon from the mode $\hat{a}_{//}$ (\hat{a}_{\perp}). Conditioning on a bad event clearly corresponds to observe the state (9) after transmission through the ABS. This does not affect its structure, but modifies its characteristic parameters as $\sigma^2 \rightarrow \sigma_t^2 = t^2\sigma^2 + 1 - t^2$, and $\delta \rightarrow \delta_t = t^2\delta\frac{\sigma^2}{\sigma_t^2}$ as a result from the extra loss.

Some manipulation leads to the final expression

$$W_{\text{ampl}}(x, p) = \frac{1}{\pi\sigma_t^2} \left(c_0 + c_1x + (c_2 + c_3x)(x^2 + p^2) + c_4(x^2 + p^2)^2 \right) e^{-\frac{x^2+p^2}{\sigma_t^2}} \quad (13)$$

where the parameters c_i are given in appendix A. We then can express the mean value of measured quadratures and show that it effectively acts as an amplifier for small amplitudes :

$$\langle X_{\text{out}}(\theta) \rangle = \frac{\sqrt{2}g\alpha \cos(\theta)\sqrt{\epsilon\eta}\xi_{\text{eff}}((1 + \delta_t)\sigma_t^2 - 1)}{(1 + \delta_t)\sigma_t^2 - 1 + \epsilon\eta(g\alpha)^2} \quad (14)$$

$$= \sqrt{\epsilon}\xi_{\text{eff}}g\langle X_{\text{in}}(\theta) \rangle + O((g\alpha)^2) \quad (15)$$

This model has been used to obtain analytic predictions about the behaviour of our device.

IV. RESULTS

The value of the input $\|\alpha\|$ is directly measured by photon counting at D_1 ; the overall detection efficiency has been previously measured by means of a well-calibrated input. It has also been checked that the input analysed with the APD and the homodyne detector gave consistent results, taking efficiencies into account.

The output state is characterised measuring 200,000 values of quadratures, sorted into 12 histograms; as explained above the data are sorted according to the a phase reference coherent with the input. For each input, we calculated the average value of the quadrature $\langle X_\theta \rangle$ and the variance V_θ relative to each phase θ ; this gives us a direct measurement of the gain and of the noise.

In Fig. 5a, we show the amplitude of the oscillations of $\langle X_\theta \rangle$ in vacuum units. We observe good agreement with the values expected from the model, except for high values of $\|\alpha\|$; we can attribute this small discrepancy to imperfect splitting ratio at the S-BS. This amplitude is then corrected for the homodyne efficiency and divided for the input amplitude, as inferred from the count rate: this gives us the measured values of the effective gain g_{eff} , reported in Fig. 5b. The agreement with our model is satisfactory; for small values $\|\alpha\| \leq 0.1$ the measured gain remains close to the set value $g=2$. This occurs despite the imperfections of the initial single photon state and of the detection: as far as the amplitude is concerned, the reduction in purity of our resource does not affect the correct functioning of the amplifier. More precisely, our model shows that for small amplitudes only the mode-matching ϵ between the single photon and the coherent state affects the effective gain.

This lack of purity shows up more clearly in the analysis of the noise, presented in Fig.6, where we can see two main effects. First, even with no input ($\alpha=0$), we observe that some excess noise is present, due to contributions from higher order emissions. Furthermore, this noise increases the non-Gaussianity of the outputs. Higher order

photons create a non-Gaussian background which is not re-gaussianified by the amplifier; this would be possible only if photon subtraction lead to the vacuum state. Purer states could be produced at detriment of the production rate by decreasing the pumping power. The results we present constitute a trade-off between these two competing requirements. In Fig.6a we report the raw data of the variance, for each input we show the minimal values ($\theta = \pi/2$), the maximal values ($\theta = 0$), and the average over the 12 histograms. In Fig 6b we report its reformulation as equivalent input noise [5], and compare it to some predictions of our model, for the experimental values of the imperfections, the ideal case with perfect single photon and mode-matching, and experimental imperfections without contributions from higher order emission.

At a difference with a coherent state, the outputs show a dependence of the variance on the observed quadrature. While this is not a signature of non-Gaussianity by itself, this derives from the truncation to the single photon term in the development (6). Therefore, the limitation to small amplitudes $\|\alpha\| \leq 0.1$ is not only necessary for a satisfactory gain, but also to reduce distortions from a symmetric shape. We can attribute the departures from our model to small drifts of the setup during the data acquisition.

The noiseless character is better understood in terms of noise equivalent power. For ordinary amplifiers this is always non negative, as the signal-to-noise ratio might at best be preserved. This is not the case for phase-independent amplifiers where there must be some excess noise, as discussed above. For large values of $\|\alpha\|$, our amplifier actually behaves like an attenuator. The corresponding deterministic deamplification is modelled as a beam splitter with transmittivity g : this deteriorates N_{eq} , as it reduces the signal without changing the noise. The corresponding curve is the dashed and dotted line shown in Fig.6b. Our points lie quite consistently under the curve when we observe amplification; in the case of deamplification, the signal-to-ratio is consistently worsened by the presence of excess noise. More strikingly, we could measure negative values of N_{eq} , which would be impossible with any deterministic device. We emphasize that this does not mean that the amplifier could improve the signal-to-noise ratio in a communication process. The key is in its non-deterministic functioning: while an enhancement occurs for the successful instances, there is no net gain if one averages on both failures and successes. The success probability P is measured as the ratio of the coincidence count rate $D_0 \& D_1$ to the single count rate D_0 : this normalizes the amplifier success rate to the single photon production. We can observe that in

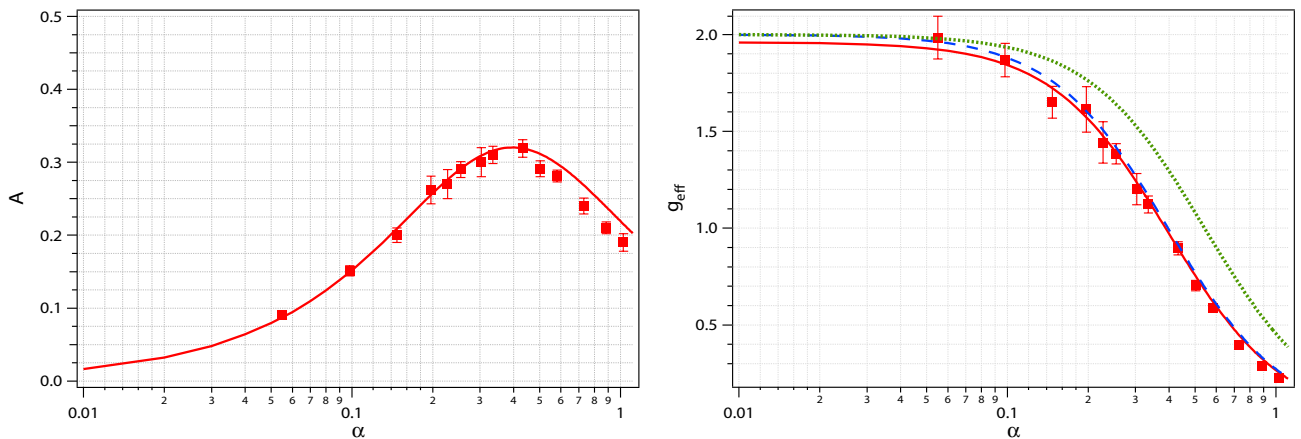


Figure 5: Experimental results for the amplification. a) Values of the amplitude of the oscillations in vacuum units; errors are indicated as the uncertainties on a sinusoid fit on the raw data. b) measured effective gain. The solid line is the prediction obtained by our model. The dotted line gives the prediction for perfect single photon and mode-matching and the dashed line gives the prediction for perfect mode-matching $\epsilon = 1$ and experimental single photon.

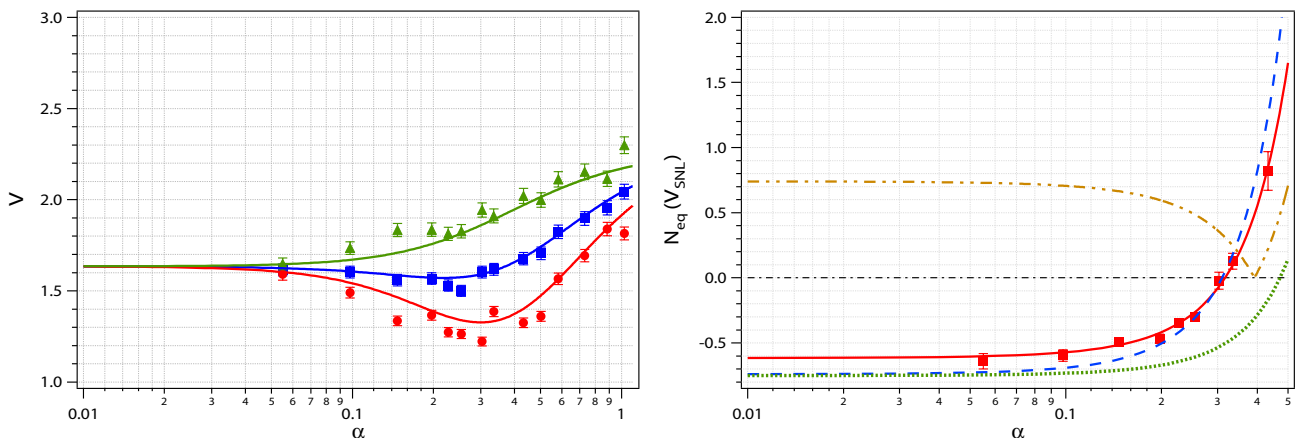


Figure 6: Experimental results for the noise. a) Values of the variance, normalised to vacuum noise: average (■), maximal (▲), and minimal (●) values. b) Reinterpretation in terms of equivalent input noise N_{eq} , only mean values are shown. The solid line is the prediction obtained by our model. The dotted line gives the prediction for perfect single photon and mode-matching and dashed line gives the prediction for experimental mode-matching $\epsilon = 0.86$ and single photon without additional parasite photons ($\sigma = 1$). The dashed and dotted line shows the minimal N_{eq} which can be obtained by a deterministic device with gain g_{eff} .

our device this increases with $\|\alpha\|$, at a difference with the ideal case, as shown in Fig.7. This is caused by the fact that we did not use conditioning on both outputs of the S-BS, and lack of photon-resolving detection. This affects the behaviour of the device at high intensities. Our model shows that the main action of photon losses, represented by δ parameter, is to reduced the success rate, while imperfect mode-matching and higher order emission increase the success probability by adding false events. The efficiency of the APD also has a significant role in success rate; since the approximation of low APD efficiency is used both in experimental setup and model we do not change this parameter in the predictions.

V. CONCLUSIONS AND PERSPECTIVES.

Our experiment provides a clear demonstration of an optical noiseless amplifier working in a nondeterministical fashion.

The possibility opened by nondeterministic amplification of coherent states have already started to inspire related works, both on the theoretical and the experimental side. Notably, an indirect and ingenious demonstration of the noiseless amplification has been demonstrated by Xiang and coworkers [23], by using photon counting and polarimetry. An alternative proposal has been put forward by Fiurášek, in the aim of coherent manipulation of light fields by photon addition and subtraction; the demonstration of noiseless amplification as a particular case of such a scheme is reported in [24]. On the same

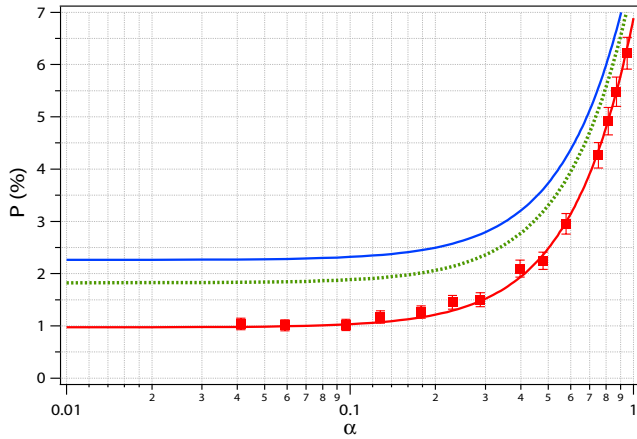


Figure 7: Experimental success probability. The solid curve indicates the prediction of our model, while the points represent the measured values. These are obtained as the ratio of the coincidences $D_0&D_1$, and the single counts on D_0 , i.e. the ratio between the successful events and all the single photon events. Dotted line gives the prediction for perfect single photon and mode-matching and dashed line gives the prediction for experimental mode-matching and single photon without losses ($\delta = 2$).

lines, schemes can be built to improve nondeterministically the signal-to-noise ratio of a peculiar task, such as phase estimation, as proposed by Marek and Filip [4], and realised by Usuga and collaborators [25].

Possible applications of our device concern quantum key distribution; a direct application could be interesting for continuous variable protocols with either Gaussian [21] or discrete phase modulations proposed, as by our group [17]. Here we put forward some considerations for the second instance. Two parties, Alice and Bob, share a set of coherent states with a random modulation with Gaussian distribution around the vacuum. We can consider the equivalent entanglement based protocol in which Alice and Bob share a two-mode squeezed vacuum (EPR state). In this case, Alice can prepare coherent states remotely at Bob's location by heterodyne measurement [22]. In this case the modulation size is measured by the variance V_B of the reduced thermal state. In order to be fully consistent, the probability must be such that the average mutual information \bar{I}_{AB} at the output does not exceed the initial value I_{AB} :

$$\bar{I}_{AB} = P \tilde{I}_{AB} < I_{AB}, \quad (16)$$

where \tilde{I}_{AB} is the mutual information of the state after the amplifier.

Some numerical results are shown in Fig. 8. We consider the case $g = 2$ with the perfect amplifier, either working in a single-stage or double-stage configuration. If we only consider the successful outputs, we notice an

increase of the degree of entanglement, thus of the mutual information between the two parties. As expected, adding more modules result in a better approximation of an amplified EPR state. When averaging on both successes and failures, the initial information I_{AB} acts as a loose bound; in fact \bar{I}_{AB} remains in both cases well under the limit value. Moreover, it is evident how increasing the number of stages does not help in recovering information, due to the unfavourable scaling of the probability with the number of stages with N . Similar results are obtained for different values of gain. In summary, the amplifier is able to produce better resources, but at a rate that does not violate any information-theoretical principle. Its realisation remains then fully consistent with information theory, while leaving open questions on its adoption for quantum cryptography. In particular, the analysis of the security is currently under process.

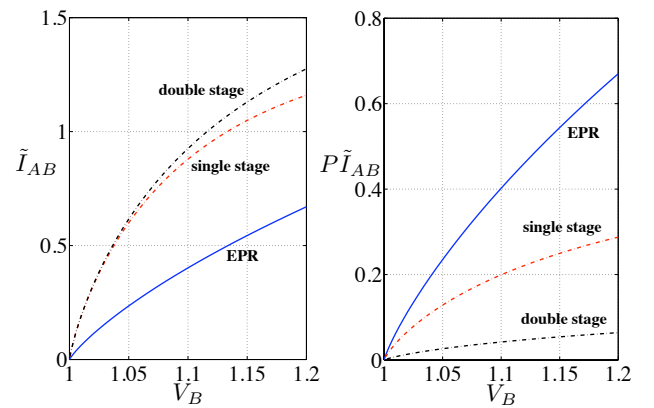


Figure 8: Mutual information between two parties in a Gaussian-modulation quantum key distribution protocol, as a function of the thermal noise at Bob's side. In the left panel we show the mutual information \tilde{I}_{AB} post-selected on the successful runs for an ideal noiseless amplifier driven at $g = 2$. The right panel illustrates the results for the average mutual information $\bar{I}_{AB} = P \tilde{I}_{AB}$, where P is the success probability.

As far as qubit protocols are concerned, the connection to device-independent quantum key distribution has been extensively discussed by Gisin and coworkers in [26].

Acknowledgements

We thank F. Fuchs, A. Ourjoumtsev, T. Debuisschert, S. Fossier, and A. Leverrier for discussion. This work is supported by the EU project COMPAS and the ANR SEQURE. F.F. is supported by C'Nano - Île de France. M.B. is supported by the Marie Curie contract PIEF-GA-2009-236345-PROMETEO.

-
- [1] C.M. Caves, *Phys. Rev. D* **26**, 1817 (1982).
[2] T.C. Ralph, and A. P. Lund, arXiv:0809.0326 (2008);
T.C. Ralph, and A. P. Lund, in *Quantum Communication Measurement and Computing Proceedings of 9th International Conference*, Ed. A.I Lvovsky, pg 155-160 (AIP, New York 2009).
[3] J. Fiurášek, *Phys. Rev. A* **80**, 053822 (2009).
[4] P. Marek and R. Filip, *Phys. Rev. A*, **81**, 022302 (2010).
[5] F. Ferreyrol et al., *Phys. Rev. Lett.* **104**, 123603 (2010).
[6] R.J. Glauber, *Phys. Rev.* **131**, 2766 (1963).
[7] F. Grosshans, G. V. Assche, J. Wenger, R. Brouri, N. Cerf, and P. Grangier, *Nature*, **421**, 238 (2003).
[8] S. Fossier, E. Diamanti, T. Debuisschert, R. Tualle-Brouri, and P. Grangier, *J. Phys. B* **42**, 114014 (2009).
[9] E. Knill, R. Laflamme, and G.J. Milburn, *Nature* **409**, 46 (2001).
[10] D.T. Pegg, L.S. Phillips, and S.M. Barnett, *Phys. Rev. Lett.* **81**, 1604 (1998).
[11] S.A. Babichev, J. Ries, and A.I. Lvovsky, *Europhys. Lett.* **64**, 1 (2003).
[12] P. Grangier, J.M. Courty, and S. Reynaud, *Opt. Comm.* **89**, 99 (1992).
[13] J.F. Roch, J.P. Poizat, and P. Grangier, *Phys. Rev. Lett.* **71**, 2006 (1993).
[14] J.P. Poizat, J.F. Roch, and P. Grangier, *Ann. Phys.* (Paris) **19**, 265 (1994).
[15] J.A. Levenson, I. Abram, Th. Rivera, P. Fayolle, J.C. Garreau, and P. Grangier, *Phys. Rev. Lett.* **70**, 267 (1993).
[16] A. Levenson, I. Abram, Th. Rivera, and P. Grangier, *J. Opt. Soc. Am. B* **10**, 2233 (1993).
[17] A. Leverrier, and P. Grangier, *Phys. Rev. Lett.* **102**, 180504 (2009).
[18] A. Ourjoumtsev, R. Tualle-Brouri, and P. Grangier, *Phys. Rev. Lett.* **96**, 213601 (2006).
[19] R. Tualle-Brouri, et al., *Phys. Rev. A* **80**, 013806 (2009).
[20] A. Ourjoumtsev, H. Jeong, R. Tualle-Brouri, and P. Grangier, *Nature* **448**, 784 (2007).
[21] F. Grosshans, G. Van Assche, J. Wenger, R. Brouri, N.J. Cerf, and P. Grangier, *Nature* **421**, 238 (2003).
[22] F. Grosshans, N.J. Cerf, J. Wenger, R. Tualle-Brouri, and P. Grangier, *Quant. Inf. Comp.* **3**, 535 (2003).
[23] G.Y. Xiang, T.C. Ralph, A.D. Lund, N. Walk, and G.J. Pryde, *Nature Phot.* **4**, 316 (2010).
[24] A. Zavatta, J. Fiurášek and M. Bellini, *Nature Phot.*, **5**, 52 (2011).
[25] M. A. Usuga, et al., *Nature Phys.* **6**, 767 (2010)
[26] N. Gisin, S. Pironio, and N. Sangouard, *Phys. Rev. Lett.* **105**, 070501 (2010).

Appendix A

The two-mode Wigner function $W_{\text{SBS}}(x, p, x_1, p_1)$ has the explicit expression:

$$\begin{aligned}
W_{\text{SBS}}(x, p, x_1, p_1) &= \frac{1}{\pi^2(\sigma^2 + \sigma_t^2)} \left(2 \left(1 - \frac{(1+t^2)\delta\sigma^2}{\sigma^2 + \sigma_t^2} \right) \right. \\
&+ \left. \frac{4\delta\sigma^2}{2\sigma^2 + \sigma_t^2} \left(\left(\sqrt{2}tx + r(x_1 - \alpha_{\text{eff}}) \right)^2 + \left(\sqrt{2}tp + rp_1 \right)^2 \right) \right) \\
&\times \exp \left[-\frac{x^2 + t^2(x - \sqrt{2}g(x_1 - \alpha_{\text{eff}}))^2 + t^2\sigma^2(gx + \sqrt{2}(x_1 - \alpha_{\text{eff}}))}{\sigma^2 + \sigma_t^2} \right] \\
&\times \exp \left[-\frac{p^2 + t^2(p - \sqrt{2}gp_1)^2 + t^2\sigma^2(gp + \sqrt{2}p_1)}{\sigma^2 + \sigma_t^2} \right].
\end{aligned} \tag{17}$$

From this formula, we obtain the coefficients for the output Wigner function

$$\begin{aligned}
c_0 &= -\xi_{\text{eff}} \frac{1 - 2\delta_t + (1 + 2g^2\alpha_{\text{eff}}^2)(\delta_t - 1)\sigma_t^2}{\sigma_t^2(2g^2\alpha_{\text{eff}}^2 + (1 + \delta_t)\sigma_t^2 - 1)} + (1 - \xi_{\text{eff}})(1 - \delta_t), \\
c_1 &= \xi_{\text{eff}} \frac{2\sqrt{2}g\alpha_{\text{eff}}(\sigma_t^2 - 1 + \delta_t(2 - \sigma_t^2))}{\sigma_t^2(2g^2\alpha_{\text{eff}}^2 + (1 + \delta_t)\sigma_t^2 - 1)}, \\
c_2 &= \xi_{\text{eff}} \frac{(\sigma_t^2 - 1)^2 - \delta_t(4 - (5 + 2g^2\alpha_{\text{eff}}^2)\sigma_t^2 + \sigma_t^4)}{\sigma_t^4(2g^2\alpha_{\text{eff}}^2 + (1 + \delta_t)\sigma_t^2 - 1)} + (1 - \xi_{\text{eff}}) \frac{\delta_t}{\sigma_t^2}, \\
c_3 &= \xi_{\text{eff}} \frac{2\sqrt{2}g\alpha_{\text{eff}}\delta_t(\sigma_t^2 - 1)}{\sigma_t^4(2g^2\alpha_{\text{eff}}^2 + (1 + \delta_t)\sigma_t^2 - 1)}, \\
c_4 &= \xi_{\text{eff}} \frac{\delta_t(\sigma_t^2 - 1)^2}{\sigma_t^6(2g^2\alpha_{\text{eff}}^2 + (1 + \delta_t)\sigma_t^2 - 1)}.
\end{aligned} \tag{18}$$

These coefficient give the predictions for the characteristic parameters of our device, in particular the effective gain:

$$g_{\text{eff}} = \frac{\sigma_t^2(c_1 + 2c_3\sigma_t^2)}{2\sqrt{2\eta\alpha}}, \quad (19)$$

and the variance

$$V_\theta = \frac{\sigma_t^2}{2}(c_0 + 2c_2\sigma_t^2 + 6c_4\sigma_t^4) - \frac{\sigma_t^4}{4}(c_1 + 2c_3\sigma_t^2)^2 \cos^2 \theta. \quad (20)$$

The quantities involved in the model are accessible from the experiment. The two parameters $\delta=0.78$ and $\sigma=1.078\sigma_{\text{SNL}}$ describing the single photon state as generated by our OPA are obtained from the variance and the fourth-order moment of the quadrature distribution of the single photon. For the output states of the amplifier, no simple relations between the momenta of the quadrature distributions and the relevant parameters has been found, so we used in our model the values of some parameters coming from direct measurements.

The transmission of the A-BS is measured by using an intense probe: it has been checked that the measured value was compatible with the values δ_t and σ_t measured in presence of this extra loss. The homodyne detection efficiency can be estimated in $\eta=0.68$ from measurements on the same probe, including a measurement of the optical loss on the path of the single photon (0.87), and of the mode matching between the probe and the local oscillator (0.90). The parameter $\xi_{\text{eff}}=0.96$ is difficult to access directly in the experiment, so it has been left as a free parameter. The detection efficiency of the APD $\eta_{\text{APD}}=0.55$ has been measured from the counts due to an intense beam, attenuated by well-calibrated neutral density filters. The overall detection efficiency is $\mu=0.11$, due to the optical loss in the path.